Astron. Astrophys. 332, 999–1016 (1998)

ASTRONOMY AND ASTROPHYSICS

Broad band infrared spectroscopy of massive young stellar objects

John M. Porter[1], **Janet E. Drew**[2], **and Stuart L. Lumsden**[3]

[1] Astrophysics Research Institute, School of Engineering, Liverpool John Moores University, Byrom St., Liverpool L3 3AF, UK
[2] Astrophysics Group, Blackett Laboratory, Imperial College, London SW7 2BZ, UK
[3] Anglo-Australian Observatory, P.O. Box 296, Epping, NSW 2121, Australia

Recieved 25 August 1997 / Accepted 24 December 1997

Abstract. We present intermediate resolution 0.9–2.5μm IR spectra of 12 highly reddened stars, including some well known and some unfamiliar sources. A new technique for extracting calibration curves from standard star data is employed, and is found to be very successful.

The reddening to each object is fully discussed and is calculated from both the continua (which was split into short- and long-wavelength regions $\lambda\lambda < 1.5\mu$m and $\lambda\lambda > 1.5\mu$m) and the HI lines. We find that, typically, there is consistency between the values derived from the HI lines and the short-wavelength continua, but not with the value from the long-wavelength continua. This discrepancy is due to an IR excess at $\lambda\lambda \gtrsim 1.5\mu$m , which is consistent with emission from hot dust (we derive dust temperatures in the range 750–1500K).

We note that some of our sources have highly discrepant Paschen decrements, and may have a significant amount of scattered light for $\lambda\lambda < 1.5\mu$m .

The spectra show a variety of metallic emission lines and some evidence for different distinct emission regions in the same source. The range of line-to-continuum contrast between the sources is high, and where previous observations have been taken, there is evidence of variability of emission line strength in some sources.

Key words: infrared: stars – stars: pre-main-sequence – dust, extinction

1. Introduction

With recent advances in IR detector array technology, the early evolution of luminous ($L \gtrsim 10^3 L_\odot$), massive ($M_* \sim 10 M_\odot$) young stellar objects (YSOs) is, once again, a topic ready for fruitful exploration. Estimates of the stellar parameters for the putative YSOs investigated here correspond to late-O or early-B type stars. YSOs generate HII regions by the action of their ionized radiatively driven winds on their natal cloud, creating cavities in the parental giant molecular cloud, appearing superficially similar to classical HII regions (see §II of Yorke 1985). Study of the spectral line emission thought to be due mainly to outflow from these young objects provides information on the early life of OB stars, and also on the evolution of the parental cloud as the mechanical and radiative energy produced by the star is fed into it.

Luminous YSOs appear as unresolved point sources at infrared wavelengths. The presence of HI recombination line emission in their spectra and the detection of free-free radio emission in many instances shows ionized gas is present. Radio spectral indices, α (defined by $S_\nu \propto \nu^{-\alpha}$), for detected sources are typically ~ 0.6 or greater, suggestive of mass loss (Wright & Barlow 1975) whereas classical and compact HII regions often have optically-thin, flat spectra ($\alpha \approx 0$) or show the optically-thick form ($\alpha = 2$). The HI recombination lines observed have widths (FWHM) corresponding to 100–300 km s^{-1} . The mass loss rates inferred from the available data are in the region of $10^{-6} - 10^{-7} M_\odot$ yr^{-1} (Simon et al. 1983, Persson et al. 1984, Beck et al. 1991). The measured expansion velocities are an order of magnitude higher than those of classical HII region recombination lines which have velocities similar to the thermal speed of the ionized gas (i.e. in the region of 10–20 km s^{-1} , eg. Bally & Lada 1983). The prototypical massive YSO is the Becklin-Neugebauer (BN) object in Orion (see Becklin & Neugebauer 1967, Bally & Lada 1983).

In its embedded phase, a massive YSO may create a compact or ultracompact HII region about itself, and is still surrounded by the remnants of its natal giant molecular cloud. The YSO's radiation will be absorbed by dust grains in the molecular cloud, and re-emitted in the IR region as thermal emission. Later in its evolution, the mass loss promoted by the luminous YSO may disrupt the natal molecular cloud to an extent that it becomes visible at optical wavelengths. In such a phase, the star might rather be classified as a Herbig Be star (Herbig 1962) than as a BN-type object. However given the relative rarity of both BN-type objects and the earlier-type Herbig Be stars it is not entirely clear what, physically, separates these two object classes (Herbig 1994) – particularly as in practice the distinction may rest primarily on reddening. Over-reliance on reddening could, very obviously, lead to an unnecessary presumption that massive YSOs placed on the far side of a molecular cloud are less-evolved than in truth they are (i.e. a YSO placed on the far side of a cloud is classified as 'BN-type', when it would be described as 'Herbig Be' if placed on the near side). A further difficulty is that it may not be correct to assume that the known Herbig Be stars are the evolved counterparts to BN-type objects. If both types of object

could be accurately placed on an HR diagram, it is conceivable they might separate out according to luminosity, with the BN-type objects intermediate between the Herbig Be stars and the young O stars powering generally more distant compact HII regions.

In order to unravel these uncertain relations it is of value both to expand the number of well-studied luminous YSOs (to achieve better statistics) and to strive for a more thorough understanding of the physics underlying the observed phenomena. Greater understanding, which can come from studying familiar sources in new ways, could facilitate more confident use of more subtle clues. The present paper is concerned with both approaches. On the one hand, our sample of 12 objects includes some relatively unknown luminous YSOs. On the other, the spectral range of the observations ($0.9 - 2.5\mu\mathrm{m}$) is significantly greater than in earlier studies at similar spectral resolution, offering the prospect of some new insights even into the familiar. We consider both the line and continuum properties of our sample and look at how these may help or confuse attempts to classify and place in an evolutionary context.

We first present the observations and describe their extraction (Sect. 2). We then go on to discuss the determination of visual extinction for each of our targets using both the continuum and HI recombination line fluxes (Sect. 3). Included in this is a discussion of particular issues raised by measurements of the individual objects. In Sect. 4 we summarise our findings with respect to spectral features produced by elements other than hydrogen. The paper ends with a discussion and the main conclusions (Sect. 5).

2. Observations and data extraction

2.1. Source selection

The target list (see Table 1) is a mixture of the familiar and the unfamiliar. The better known sources include GL 961, R Mon, M8E, M17 SW and MWC 297 (eg. Persson et al. 1984, Simon et al. 1983, Kelly et al. 1994, Hillenbrand et al. 1992, McGregor et al. 1984, Bunn et al. 1995). As well as adding to the sum of knowledge on these objects, our data on them may usefully be compared with earlier data sets. Much less is known about the IRAS sources and LSS 3027B. Beck et al. (1991) obtained large aperture observations of the Brα, Brγ and Pfγ HI line emission of some of the IRAS sources after their identification as possible YSOs by Persson & Campbell (1987). Beck et al. estimated mass loss rates on the basis of a schematic wind model for the line emission, and also derived luminosities, distances and extinctions for the sources. LSS 3027B has received even less attention - Steenman & Thé (1989) identify it as a Herbig Be star candidate, but do not elaborate on this hypothesis.

2.2. Data acquisition and extraction

The data were obtained using IRIS, the infra-red imaging spectrometer on the Anglo-Australian Telescope on the nights of 22^{nd} and 23^{rd} March 1994. IRIS has a 128x128 pixel Rockwell HgCdTe array, with each pixel corresponding to 0.8 arcsec on the sky. The slit width was set to 2 pixels wide or 1.6 arcsec for every observation. The seeing was measured at between 2–2.5 arcsec in the near infrared for both nights. Each target was observed with both IJ and HK echelles to obtain complete wavelength coverage between 0.9 and 2.5μm. Atmospheric standard star observations were obtained both preceding and following each target observation. The standards matched the target observations to within $\sim$0.1 in airmass. The wavelength resolution achieved is $\lambda/\delta\lambda \sim 400$, which corresponds to 40Å at a wavelength of $1.6\mu\mathrm{m}$. In most cases both object and target were observed by nodding along the slit to provide sky subtraction. For the more extended objects we nodded off to blank sky. The slit was oriented east–west in all observations.

Since IRIS presents echelle orders that are curved on the array, these had to be remapped first to straighten them. The positive and negative nod positions were then extracted from the image and subtracted from each other to give a final sky subtracted spectrum. The number of rows extracted varied with the target under consideration: the effective beam size for each object is shown in Table 1. The individual orders were merged together to yield the complete spectrum: the IJ orders were scaled to the HK orders where the two overlap. Absolute spectrophotometry is not possible because of the limited slit width. However, relative photometry was achieved allowing the determination of relative line fluxes and the shape of the spectral energy distributions. The wavelength range covered straddles two atmospheric absorption bands at 1.3-1.45$\mu\mathrm{m}$ and 1.8–2.0$\mu\mathrm{m}$ which have been cut out of the data. Wavelength calibration was from an argon arc lamp.

Terrestrial atmospheric absorption was corrected for and relative flux calibration achieved using Kurucz (1991) model atmospheres (in place of the conventional method of adopting blackbody temperatures). Appropriate atmospheres were selected for the standard stars according to the stars' colours and spectral types, and these were divided into the standard star data to obtain calibration curves. The standards used have a range of spectral types from B9–F6. One problem encountered with the available grid of Kurucz atmospheres is that the spectral resolution changes in the wavelength region considered from $\delta\lambda = 20$Å for $\lambda < 1.0\mu\mathrm{m}$, up to $\delta\lambda = 50$Å for $1.0\mu\mathrm{m} < \lambda < 1.6\mu\mathrm{m}$ and then to $\delta\lambda = 100$Å for $\lambda > 1.6\mu\mathrm{m}$. Comparing this resolution with the resolution of the object spectra (~ 40Å), the Kurucz atmospheres were inadequately sampled for $\lambda > 1.0\mu\mathrm{m}$. This presents no problem with regard to the continuum extraction, but it is insufficient for the correct extraction of the HI Brackett lines. To deal with this, the lines in both the standard star observations and the model atmosphere were cut out and replaced by interpolated continuum. These manipulations were performed using the STARLINK software package, DIPSO.

Most source spectra could be calibrated against two standard stars, allowing a comparison to be made between the separately derived results. For those sources which were observed on both nights, a comparison could also be made between the final source spectra for each night. We found this modified prescription for extracting IR spectra to be very stable *both* between standards for the same object *and* between nights for the same

Table 1. Source list in RA order. Where more than one exposure time is entered in the IJ column, the source was observed twice and each figure is the total for each night.

Source	RA	Dec	total exposure time		Beam Size
	(1950)	(1950)	IJ (s)	HK (s)	arcsec^2
GL 961W	06 31 58.8	+04 15 08.4	1800	1200	9.0
GL 961E	06 31 59.1	+04 15 09.5	1800	1200	7.7
R Mon	06 36 26.05	+08 46 54.5	720,900	480	12.8
IRAS 07173-1733	07 17 22.28	-17 33 42.6	1440	960	10.2
IRAS 09014-4736	09 01 27.39	-47 36 34.8	1440,1440	720	8.3
IRAS 12389-6147	12 38 58.10	-61 47 49.7	1200,1120	576	10.2
LSS 3027B	13 15 51.5	-62 17 58	2880	960	9.0
IRAS 14206-6151/1	14 20 37.70	-61 52 10.4	2400	1440	9.0
IRAS 17441-2910	17 44 08.91	-29 10 53.1	1440	720	10.2
M8E-IR	18 01 48.8	-24 26 56	960,1440	288(H),240(K)	9.0
M17SW IRS1	18 17 26.5	-16 14 54	2240	720	9.0
MWC 297	18 25 01.2	-03 51 46.3	240	64	11.5

source (differences in the flux are at the $\lesssim 5\%$ level over most of the wavelength range). This leads to a high level of confidence in the quality of the relative spectrophotometry achieved. We also checked the results of this technique against the standard method of assuming the standard star is a black-body. We found essentially no difference for $\lambda > 1.3\mu$m, but that at shorter wavelengths the observations normalised using Kurucz model atmospheres are noticeably bluer (by up to $10-20\%$ at 8500Å) as might be expected given the range of spectral types chosen for our standard stars.

3. Results

The spectra of all of the target stars (Fig. 1) rise towards the red through most of the observed wavelength range. The hydrogen Brackett series are obvious in all spectra except one (IRAS 14206-6151/1, Fig. 1), as are some of the lower members of the Paschen series (Paβ, Paγ, Paδ). Many of the sources exhibit OI lines, and also FeII lines. There is evidence for the CO bandheads being in emission in some of the sources, although the line-continuum contrast is too small to make reliable flux measurements in certain instances. All line flux measurements, expressed relative to Brγ, are set out in Table 2.

The wavelength range between 0.9μm and 2.4μm contains enough data to determine the reddening to each object by two different methods; from (i) continuum shape and (ii) ratios of hydrogen recombination line fluxes. We discuss dereddening carried out by these means in describing the continuum and HI line characteristics of our targets below (Sects. 3.1 and 3.2). The reddening and HI emission line properties of the individual targets observed are reviewed in Sect. 3.4, and summarised in 3.5. Finally, in Sect. 3.6, we survey the HeI and heavy element lines present in the spectra.

3.1. Continuum emission

In order to derive the reddening of the objects from their continua, the intrinsic flux distribution needs to be known. Using the assumption that the unreddened stars are all of early type, the flux distribution between 0.9 and 2.4μm will be similar to the Rayleigh-Jeans tail ($f(\lambda) \propto \lambda^{-4}$). Inspection of model energy distributions suggests that deviations from this curve for a 30,000K near main-sequence star are only of order 10%, rising to 25% for a 15000K star. All the objects are likely to have late O or early B spectral types since they are the exciting sources of the HII regions, but exhibit little HeI emission. Hence in dereddening the observed continua to the Rayleigh-Jeans form, the likely error is small, amounting to no more than 0.05–0.1 magnitudes. The judgement that sufficient dereddening had been applied to a spectrum was made by eye. The error in this practical step is far greater, being on the order of 3 magnitudes in $A_{\rm v}$. The extinction law used to deredden the spectra is that due to Howarth (1983).

In view of the significant likelihood that excess IR emission might be present in all or some of our targets, the continuum dereddening has been performed in two distinct wavelength regimes: $0.9\mu{\rm m} < \lambda \lesssim 1.5\mu{\rm m}$ and $1.5\mu{\rm m} \lesssim \lambda < 2.5\mu{\rm m}$. The first wavelength range will be less contaminated by any circumstellar material, and so should typically give a more reliable evaluation of the reddening. However, in this region the observed flux is lower and so the noise in the spectra will be amplified in the reddening determination.

The longer wavelength range can be dominated by excess emission which causes the de-reddening (to yield an intrinsic Rayleigh-Jeans spectrum) to suggest a very much higher visual extinction than is needed at shorter wavelengths. In effect, a significant difference between the reddening determinations provided by the two wavelength regions is evidence of an excess due to circumstellar emission setting in at 1–2μm. The visual extinctions derived from the continua are tabulated in Table 3. An estimated extinction is only quoted for the longer wavelength range in those cases where the increase on the $\lambda < 1.5\mu{\rm m}$ figure is no greater than $\sim 2\sigma$. The spectra obtained on dereddening using the extinction derived from the shorter wavelength continuum are shown in Fig. 2. From these it can be seen that in several cases, the IR excess becomes apparent just longward of 1.1 or 1.2 μm. Because of this, the A_v derived from long-wavelength part of the spectrum is a poor estimate of the true extinction.

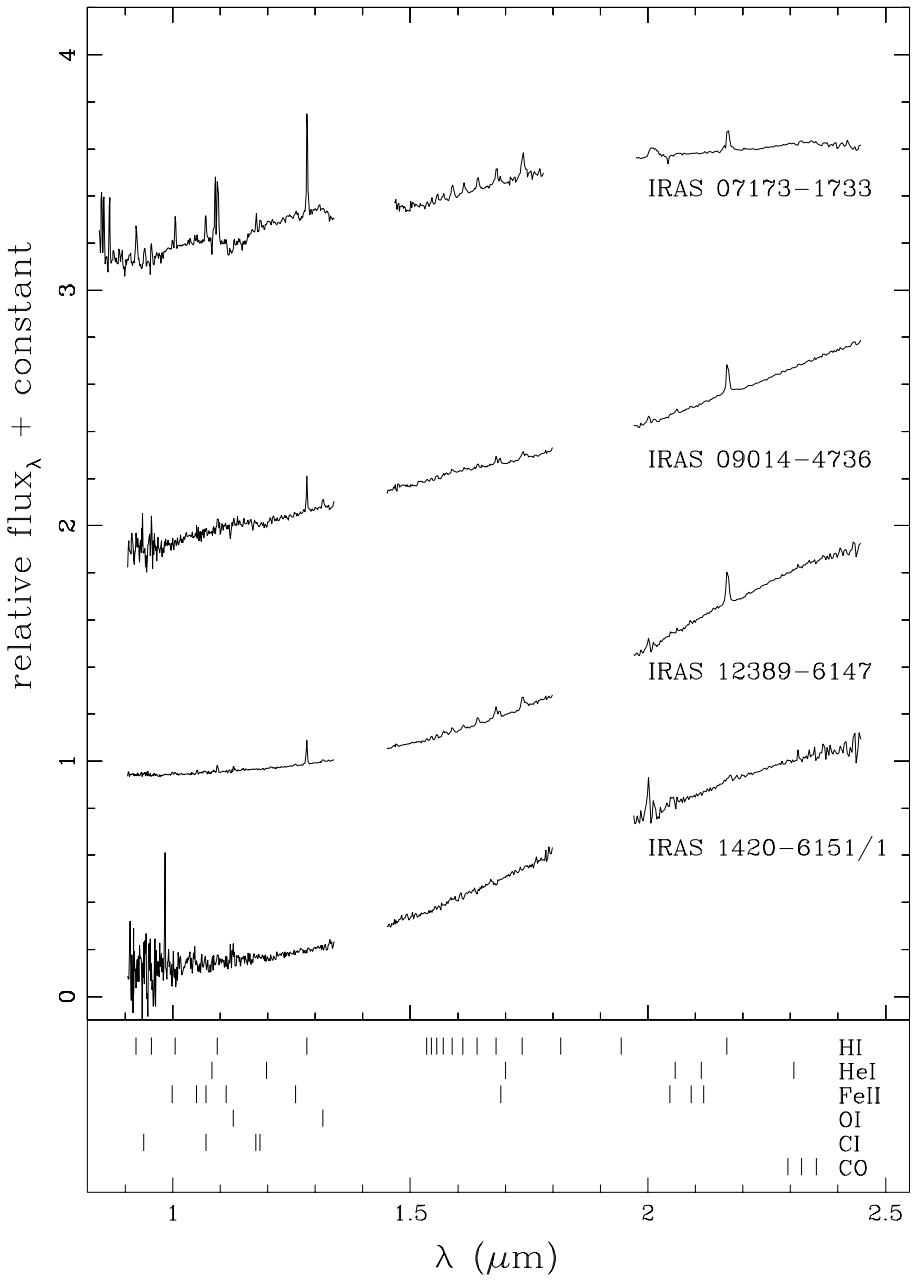

Fig. 1. Calibrated 0.9–2.4μm spectra. The flux scale should be understood to be per unit wavelength (i.e. f_λ rather than f_ν)

3.1.1. Origin of the continuum excess

The assumption that the inherent flux distribution roughly follows a Rayleigh-Jeans tail does not cater for any excess IR emission local to the star. In truth, we can expect many (if not all) to exhibit an excess continuum component somewhat longward of 1μm . Our targets are thought to be young and in the present paradigm of star formation, protostars grow through accretion of material in their equatorial plane (see Shu, Adams & Lizano 1987 and Yorke 1985). If the objects observed have not dispersed their natal dusty discs and envelopes, then there is the potential for excess IR radiation.

Dust is destroyed at temperatures of $\gtrsim 1500$K and so is likely to be emitting at a lower temperature in YSO environments. McGregor et al. (1988) calculate dust temperatures around their sample of early spectral type emission-line stars and find dust temperatures varying between a few 100K and the sublimation temperature. By comparison, the dust temperature observed around a normal HII region is typically ~ 750K (Lumsden & Puxley 1996). The wavelength of maximum emission for a grey body at 750K temperature with power law exponent of unity (typical of warm dust emission at short wavelength) is $\sim 5\mu$m . However, it is characteristic of Herbig AeBe stars to show an IR excess that becomes noticeable between 1 and 2μm, and peaks at about 3μm. This is well-documented in the survey of Hillenbrand et al. (1992) and has been discussed by Lada & Adams (1992) and by Hartmann, Kenyon & Calvet (1993). If this shorter-wavelength emission is due to dust, it could very well be non-thermal in origin. A likely mechanism is "spiking"

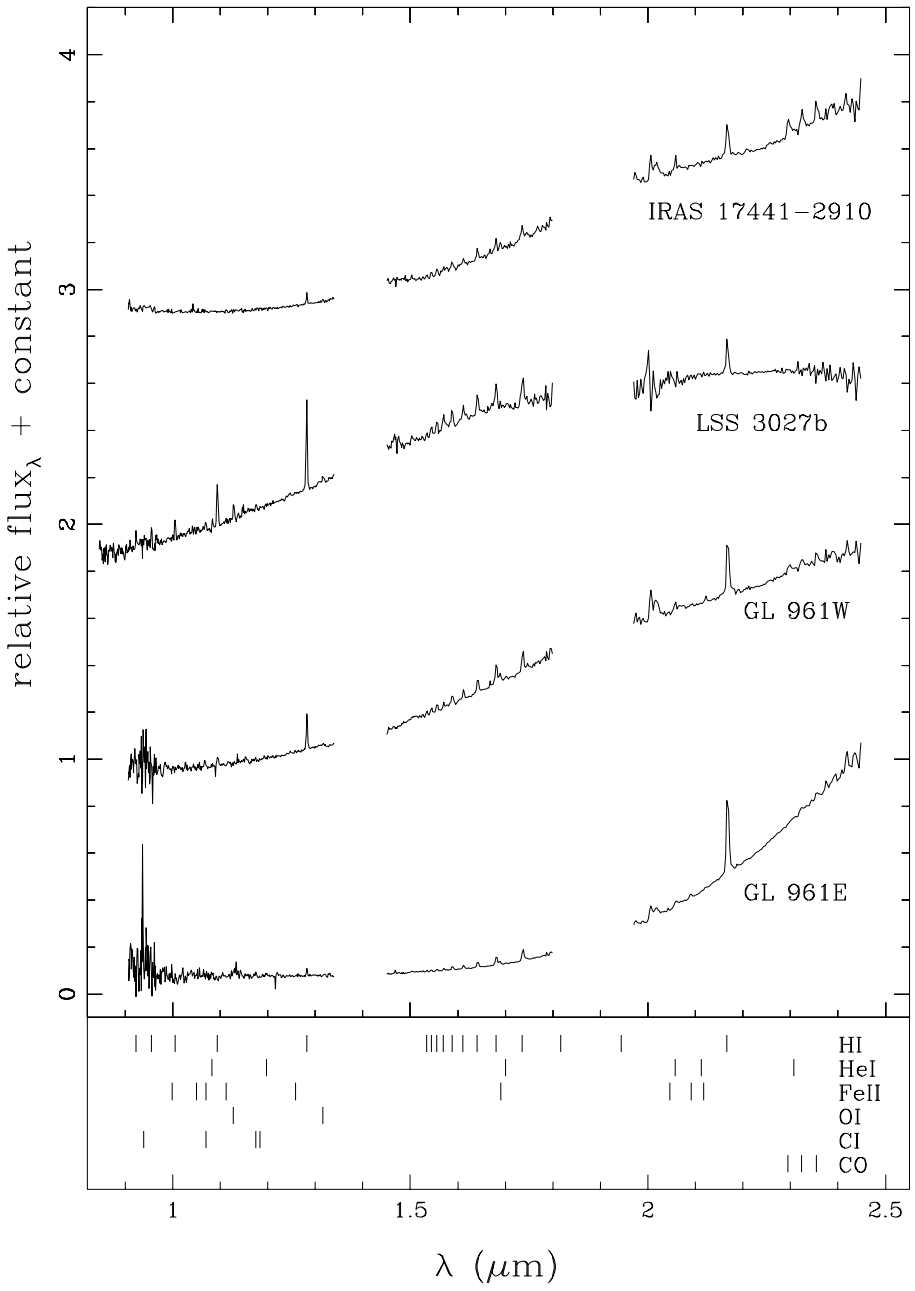

Fig. 1. (continued)

by small grains – small grains have a low thermal capacity, and so when they absorb an ultraviolet photon, their temperature increases sharply until it re-radiates the energy away as near IR photons (see Guhathakurta & Draine 1989).

In addition to the component of reddened starlight, we consider three further components that, in principle, might contribute to the observed continuum emission. First, optically thin free-free and bound-free emission may be present. We can derive an approximate measure of the importance of this contribution from the measured equivalent width of Paβ. For conditions in which optically-thin emission is likely to arise ($T_e = 7500$K, $N_e \sim 10^3$cm^{-3}), the equivalent width is expected to be 0.15μm. We do not measure an equivalent width as large as this in any of the objects. In practice, even in GL961E, the object most like a standard HII region, the equivalent width is too low by a factor of 20. It is clear that the hydrogen continua are unimportant in explaining the overall features of these sources. The lack of evidence for the Brackett or Pfund breaks being present is also a strong indicator or the relative lack of importance of bound-free and free-free emission. We therefore exclude this component from further consideration.

The second likely source of continuous emission, as mentioned already, is hot dust, which we can model (crudely) as a grey body at a temperature T_d (i.e. $f_\lambda \propto \lambda^{-\alpha} B_\lambda$). We only accept as plausible the parameter ranges $500 < T_d < 2500$K and $0 \leq \alpha \leq 2$. In practice α and T_d are highly correlated, so we cannot say much about the exact nature of the dust emission, but it is clearly present to some extent in many of our targets.

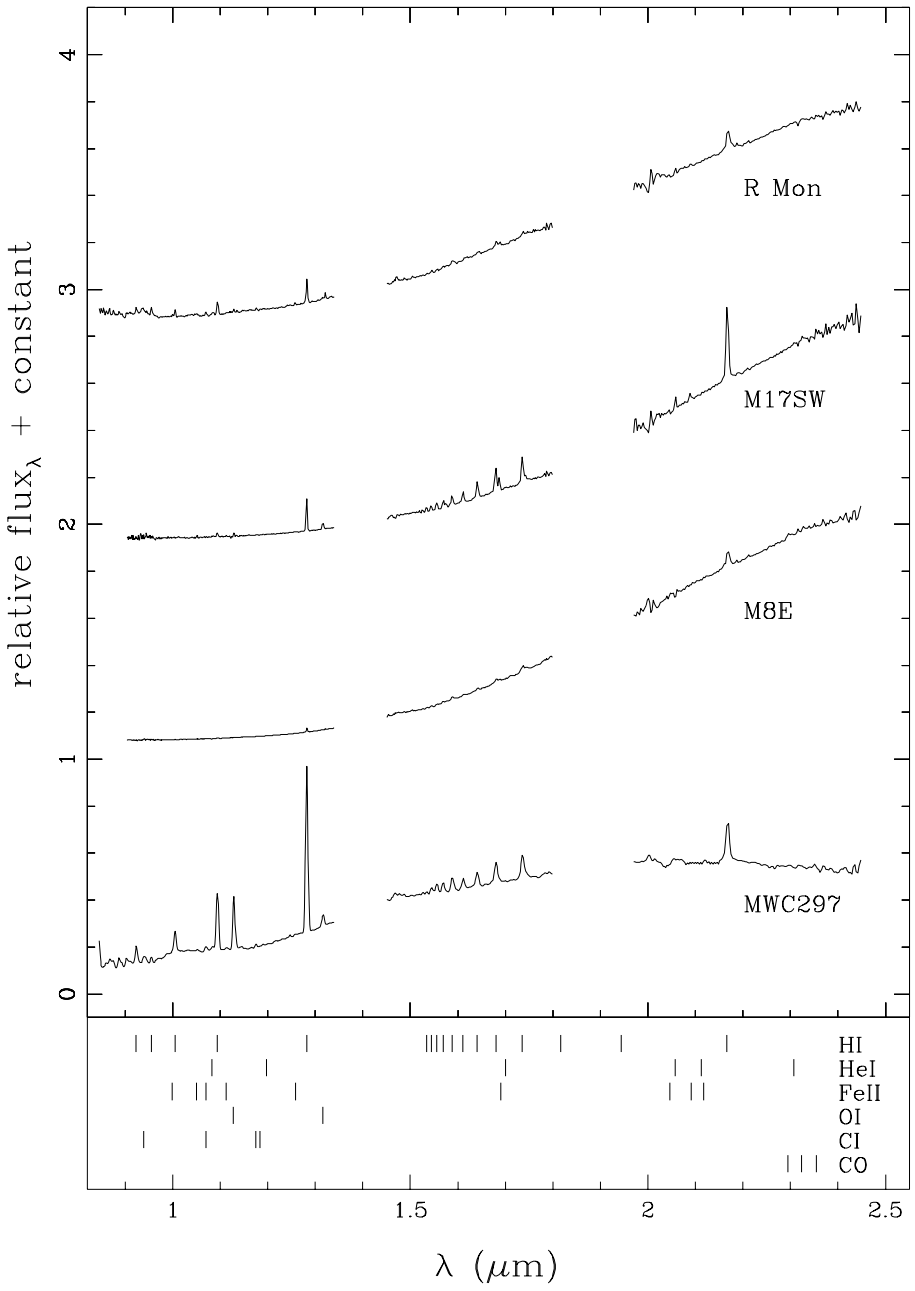

Fig. 1. (continued)

Lastly, it should not be overlooked that there could be optically thick emission from an ionised stellar wind. We note that this typically creates much more modest excesses than those due to dust and, as its spectral shape is not so simply parameterised, we do not include it in our fits to the data.

Our procedure for assessing the dust component was as follows: we dereddened the data using the observed starlight component for $\lambda < 1.5\mu\mathrm{m}$, as described above, and then found a match to the whole spectrum by varying the parameters of the dust contribution. We did not formally fit the data since many of the parameters are correlated and the exact minimum of the fit is therefore fairly shallow. As we are only interested in general behaviour, it was sufficient to estimate the best fit by eye. It should be noted that this treatment of the data involves the assumption that both the starlight and the excess IR emission are reddened to the same extent. This is probably a reasonable approximation for the deeply embedded sources, but becomes more questionable for the least reddened.

The objects can be grouped into four categories. The first category contains only GL961E, which can best be described as a relatively normal HII region. The continuum is well described by a combination of reddened starlight and moderately hot dust ($T_d \sim 750$K), mostly independent of α. The behaviour of this object is very similar to the compact HII region G45.12+0.13 studied in Lumsden & Puxley (1996), with the exception that the latter shows a more obvious hydrogen bound-free and free-free continuum. Given the lack of evidence for any helium recombination lines in the spectrum of GL961E, it is likely that the

differences can be explained purely in terms of the effective temperatures of the exciting stars, with GL961E only containing B stars whereas G45.12+0.13 contains stars with effective temperature at least as great as 40000K.

The second group contains the bulk of the objects. These have properties that are extreme, but do not necessarily require components other than dust to explain their IR excesses. Typically, reddened starlight plus dust near the sublimation temperature gives a good fit. The objects in this class are R Mon, GL961 W, IRAS 07173-1733, IRAS 09014-4736, IRAS 12389-6147 and M17 SW. The power law exponent of the dust is relatively insensitive to the data being fitted (although T_d changes by $\pm$300K as the grey body component increases from a pure black body to $\alpha = 2$). The derived T_d is typically high (~ 1500 K), but not beyond the likely range of dust sublimation temperatures, and the emissivity index, α is of order unity.

The third category includes IRAS 14206-6151/1, M8E-IR, LSS 3027B and MWC 297. Again, dereddened starlight adequately represents the blue data, but here any fit to the red end of the spectrum using a grey body gives results that are inconsistent with expectation ($T_d > 2000$K and $\alpha \geq 2$). Optically thick emission from the gaseous outflow may be a more than usually significant if not necessarily dominant contribution to the IR excess in these objects. Indeed in MWC 297, a relatively nearby object, there is a resolved but nevertheless fairly compact source of thermal radio emission (see Drew et al. 1997) in keeping with this.

Lastly, IRAS17441-2910 appears to have very little IR excess. Judged on this alone it would appear to be describable as a reddened star.

3.1.2. Hydrogen line fluxes

A second commonly used method for determining extinctions is based on measurements of hydrogen recombination line fluxes. These lines are assumed to form in a region lying behind a foreground blanket of interstellar and/or circumstellar dust. If Case B recombination is assumed to apply, then the intrinsic ratio of the fluxes of two lines can be calculated (Hummer & Storey 1987) and compared with observed ratios.

We select only those HI lines for which we have confidence that their relative line fluxes are unaffected by blending or calibration problems. These are Brγ, Br10–12, Br16–18, Paβ, Paγ and Paδ, although for some objects the Paschen series could not be measured beyond one of Paγ, or Paβ (see Fig. 3). To each line measured the following procedure is applied: (i) the line flux of Brα is estimated from the observed flux using the intrinsic case B line ratio (calculated at temperatures of 10^4K and densities of $\sim 10^4$cm^{-3}), (ii) this flux is then plotted versus $A_\lambda/A_v = (\lambda/0.6)^{-1.7}$ (Koornneef's 1983 reddening law). If the lines are formed as in Case B recombination theory, the points plotted should fall on a straight line, the gradient of which will be the visual extinction A_v. The plots obtained this way are shown in Fig. 3, and the derived visual extinctions are included in Table 3. The errors in the determination of A_v are derived from the least-squares fit to the points in Fig. 3, are also given in the table.

We note that for three of our brighter, less reddened objects, we were able to measure the Pa-11 relative line flux. However, as is apparent in Fig. 3, this line is curiously discrepant with respect to the other Paschen lines. We suspect that this is a product of a systematic calibration problem connected with the convergence of the Paschen series in our standard stars. It is for this reason that we only plot the Pa-11 points in Fig. 3, and have not included them in the extinction fits.

Ultimately the reliability of this method depends upon the extent to which Case B recombination is a fair representation of the intrinsic line flux ratios. In every case the Brγ line seems to have a smaller flux than is consistent with the general trend, something also seen by McGregor et al. (1984). This is very likely to be due to significant optical depths in the line forming region, resulting in deviations from Case B recombination theory (see Thompson 1982 and also the discussion). In several instances it is also seen that Paβ falls too low as well. Accordingly, it may seem better to weight the higher series lines more in the extinction determination rather than the strongest and lowest series members observed. In fact, if optical depth is causing the $n = 3$ and $n = 4$ levels of the hydrogen atom to be enhanced relative to their Case B values, $n = 3$ will be affected more, causing the Paschen lines to underpredict the corresponding Case B Brα flux (i.e. in Fig. 3 all the Paschen points will sit relatively low, regardless of their optical depth). Because of this, it is reasonable to expect the trend between the higher Brackett lines and the highest member of the Paschen series that is measurable to be steeper than if Case B strictly applied. We might expect, therefore, a tendency to overestimate the extinction. Perversely, inclusion of Brγ in the slope determination may help to counter this!

In short, there is no simple way to correct an extinction estimate for the effects of deviations from pure Case B recombination. But there is reason to hope that these might crudely cancel if enough lines are considered. Furthermore, at high A_v deviations from Case B recombination will be proportionately less important. The test of this is to make comparisons with independently-derived extinction estimates – in this instance we compare with the continuum method. This exercise turns out to be surprisingly successful. When comparing our values to previously published estimates, we find a good degree of agreement. However, for three sources the reddenings derived from the HI lines are seriously discrepant. For these sources, the extinctions calculated from only the Paschen lines are consistant with those quoted in the literature, which are also derived from the short wavelength region (see §3.2.1, §3.2.6 & 3.2.8), a wavelength-dependant phenomenon which has been highlighted previously (see Close et al. 1997).

3.2. Notes on individual targets

Below, the hydrogen line spectra and extinction determinations are presented for each object in turn, beginning with the less well known of our targets.

Table 2: Line fluxes normalized to Brγ. "p" indicates that a particular line is present, although difficult to measure due to continuum fitting porblems: "?" indicates that the line may be present: "b" indicates that the line is blended. ":" indicates that the measurement is uncertain. The 1.741μm FeIIand 1.737μm Br10 lines are blended where the 1.741μm FeIIline is indicated as present.

λ	ID	IRAS	IRAS	IRAS	IRAS	IRAS	LSS3027b	GL961W	GL961E	R Mon	M17SW	M8E	MWC297
μm		0717	0901	1238	1420	1744							
2.354	CO(4-3)					56		7					
2.324	CO(3-1)					59		10					
2.295	CO(2-0)					57		14				40:	
2.2124												8	
2.2087	NaI	5	?	?		10		?		p	?	?	
2.1657	Brγ	100	100	100	100	100	100	100	100	100	100	100	100
2.113b	HeI												
2.091	FeII		2	?									
2.0583	HeI		3	6		25		13	9		9	?	
1.741	FeII	p	p	p					p		p	p	
1.7370	Br10	70	9	35		49	77	25	12	18	34	37	57
1.7011	HeI												
1.6873	FeII	p	6	9		12		14	3	9	5	6	
1.6812	Br11	42	11	28		34	69	27	8	12	24	25	43
1.6414	Br12	26	12	17		19	50	16	5	10	16	9	32
1.6117	Br13	33	13	10		16	54	12	4	12	11	5	18
1.5888	Br14	42	12	10		14	37	12	3	16	9	12	22
1.5766			4							4	1	2	
1.5708	Br15	30	6	12:		15	42	6	2	7	5	5	12
1.5562	Br16	34	4	5		7	21	6	1	4	5	4	11
1.5444	Br17	21	3	5		4	19	4	p	5	4	3	6
1.5345	Br18	9	3	3		4	9	3	p	2	3	4	5
1.5266	Br19			1							1	2	4
1.3274	[FeII]			p									
1.3166	OI		16	3		p	11	?		2	5		19
1.2818	Paβ	128	48	31		14	133	34	3	44	24	9	268
1.2566	[FeII]			2				?		4	?		
1.247	NI							?					3
1.1848	CI	10										?	1
1.175	CI	20					7			3		?	4
1.1287	OI	p		9			21			4:	2	?	72

Table 2: continued.

λ	ID	IRAS	IRAS	IRAS	IRAS	IRAS	LSS3027b	GL961W	GL961E	R Mon	M17SW	M8E	MWC297
μm		0717	0901	1238	1420	1744							
1.0945	Paγ	104	33	7			51	7		20	2	2	83
1.091	HeI/MgII	95											
1.0830	HeI	-22					6			7			4
1.070	CI/FeII	57					11	6		6			6
1.051	FeII?	9		5							1		p
1.040	[NI]/FeII	10											
1.0055	Paδ	44		2			25			9			30
0.9995	FeII	9		2						3			
0.9545	Pa8	24	22				26			11			10
0.9455	NI?									3			5
0.9406	CI	35											
0.9395	NI/FeII												8
0.9365			23							20:			
0.9233	Pa9	110					20			13			31
0.9095	CI									6			
0.9014	Pa10												11
0.8924		11								7			
0.8863	Pa11	18								5			14
0.8750	Pa12	21								6			7
0.866	Pa13/CaII	91								8			15
0.8598	Pa14									3			5
0.8542	Pa15/CaII	93								7			4
0.8498	Pa16/CaII	101								7			5
0.8446	Pa17/OI	74								7			

Table 3. Visual extinction derived for each object in magnitudes. The values appearing in brackets derived from the HI lines are obtained on including the Pa11 relative flux (see text). The error in A_v for the continuum is $\pm$3mag. Superscripts refer to the following references: (1) Hillenbrand et al. ,1992 (2) Beck, Fischer & Smith, 1991 (3) Simon et al. , 1985 (4) McGregor, Persson & Cohen, 1984 (5) Kelly, Rieke & Campbell, 1994 (6) Steenman & Thé, 1989 (7) Alonso-Costa & Kwan, 1989 (8) Cohen & Kuhi, 1979

Source	A_v H lines	A_v $\lambda < 1.5\mu$m	A_v $\lambda > 1.5\mu$m	A_v from other studies	
IRAS 0717	9(8)$\pm$2	9		2^2	
IRAS 0901	13$\pm$2	13		26^2	
IRAS 1238	20$\pm$2	19		21^2	
IRAS 1420	-	23	30		
IRAS 1744	27$\pm$3	31	34		
LSS 3027B	13$\pm$3	13	20	5.97^6	
GL961 W	21 ± 3	20	28	28 ± 4^7	15.3^4
GL961 E	25 ± 3				
R Mon	12(9)$\pm$1	10		3.6^5	4.2^8
M17SW IRS1	26$\pm$3	27		14.5^4	18 ± 4^7
M8E-IR	28$\pm$4	24		21^3	15^4
MWC 297	9(7)$\pm$1	8		8.3^1	7.9^4

3.2.1. IRAS 07173-1733

Persson & Campbell (1987) included this source in their catalogue of YSO candidates derived from 2.1-2.4μm spectra and IRAS fluxes.

Beck et al. (1991) identify IRAS 07173-1733 as a star with a wind, relatively close to emerging from its natal cloud – the extinction they derived was $A_V \simeq 2$. Our observations are at variance with this in favouring $A_V \simeq 10$. However, we are encouraged to find agreement between the extinctions derived separately from the HI lines and the $\lambda\lambda$s $< 1.5\mu$m continuum – a pattern repeated in practically all of our targets.

How may we understand the clear discrepancy between Beck et al. 's (1991) extinction estimate and ours, given that both exploit recombination line ratios? Beck et al. use an intrinsic Brγ/Pfγ flux ratio given by a wind model due to Smith et al. (1987) in which it is predicted that Brγ/Pfγ= 3.5 for a wide variety of outflow parameters. This is not so different from the Case B value of 2.8 that it can be the explanation. The difference may, instead, be due to the difficulty of measurement of very weak Pfγ emission in this source's spectrum (extracted by Beck et al. using a maximum entropy technique). We note that the error they estimate for the raw spectrum is actually greater than the line they 'detect' from the maximum entropy method.

Persson & Campbell (1987) measured the equivalent width of Brγ to be 5 ± 2Å and Beck et al. measure a value of 3.8 ± 0.6Å. The former is compatible with our result of 6 ± 1.5Å, though the latter is only just so. Some comments must be made about these earlier measurements. Both groups used large aperture (10 arcsec diameter for Beck et al. , 8 arcsec diameter for Persson & Campbell) detectors utilising either a single photometer and a CVF (Persson & Campbell) or a grating plus linear detector (Beck et al.). It is therefore possible that if the continuum is more extended than the line flux, they would measure a lower equivalent width. We can test this effect using our data. Although we do not have spectrophotometric data, we are able to estimate crude magnitudes assuming that both object and standard behave as point sources. From this we find that our data agrees with the photometry of Persson & Campbell to within 0.3 magnitudes for all sources apart from IRAS 17441-2910, a difference easily explained by the crudity of our 'flux calibration'.

A more important likely source of difference between our values and those of Persson & Campbell and Beck et al. is the change in spectroscopic technology. First, given the observing procedure with a CVF (Persson & Campbell 1987) is to step through in wavelength, there is an obvious difficulty in detecting weak lines. A conservative lower limit on possible detections is to assume that, if conditions were perfect and the instrument functioning well, it may be possible to detect a line which contributes only 1% of the flux in a given bin by comparison with its neighbours. This can be translated easily into a limiting equivalent width, using the instrumental resolution (set by the 1.25% bandpass of the CVF), to give a limit of ~ 2Å. This value may be $2-3$ times larger in practice. Persson & Campbell often quote errors on the equivalent width equal to or smaller than this – these should be regarded as very optimistic. The measurements of the Beck et al. data, should be more reliable, since the resolution was higher (allowing a greater line to continuum contrast) and the detector had eight elements allowing continuum and line to be sampled simultaneously. However, the object had to be scanned repeatedly with the wavelength shifted in order to fully sample the spectrum. Beck et al. used three sub-samples to create their final spectra. This procedure can easily lead to spurious baseline errors when the sub-spectra are coadded. This leaves open the possibility that the baseline calibration of the Beck et al. data may be slightly suspect.

Despite these observational considerations, it could still be the case that the hydrogen line emission or indeed the continuum is slightly variable. Only repeat observations using similar instrumentation can verify this.

In Fig. 3, it can be seen that the Brackett lines display a large scatter, and that it is particularly striking that the Paschen lines alone give the impression of negligible reddening for this

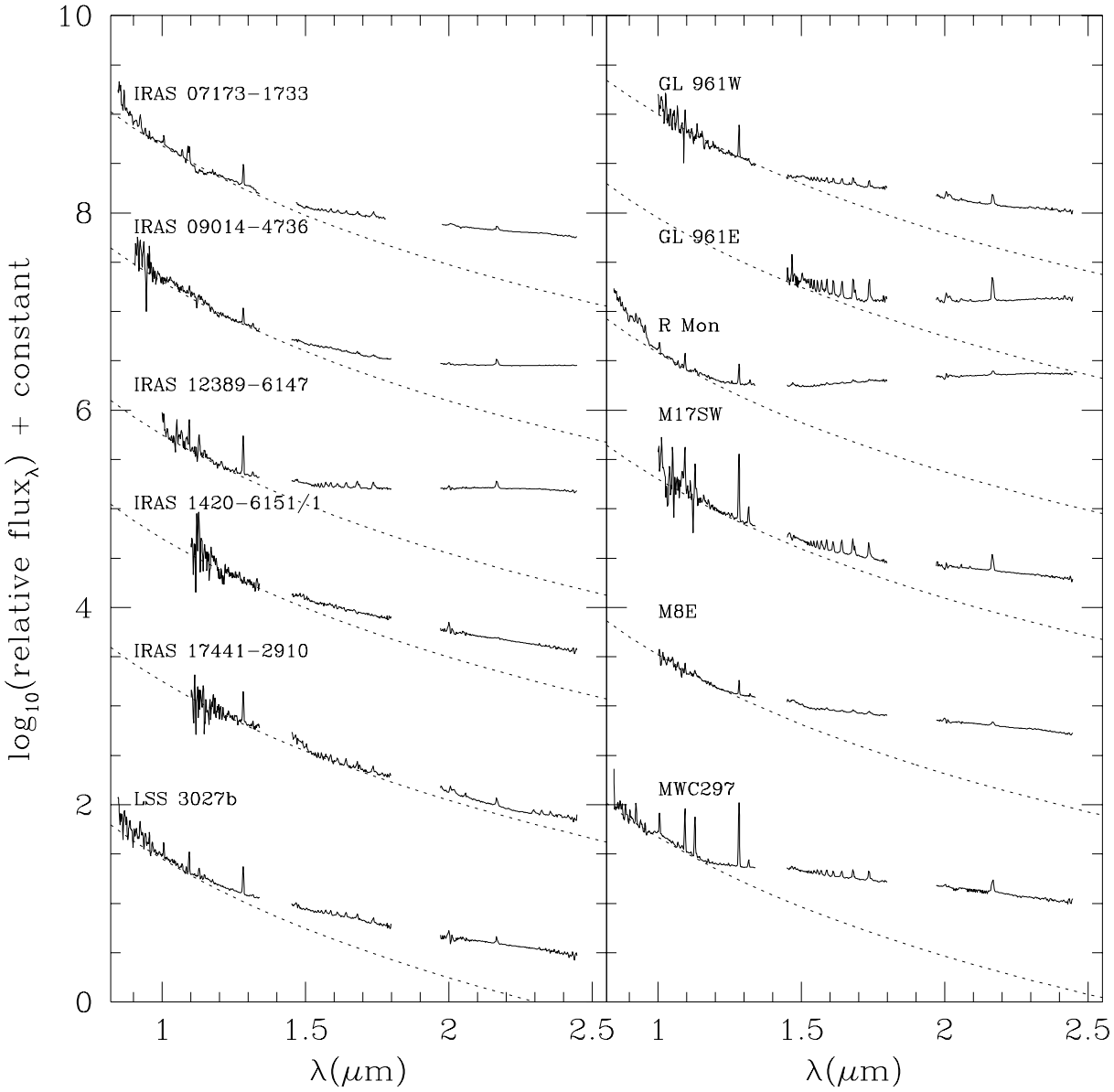

Fig. 2. The spectra after dereddening using the extinction derived from the short wavelength continuum. In each panel the Rayleigh-Jeans shape is plotted as a dotted line.

source. The same phenomenon is observed in all but one of our sample of objects for which measurement of Paδ is feasible (see below). The figure for IRAS07173-1733 of $A_v \simeq 10$, owes its origin to this contrast between the Brackett and Paschen series.

3.2.2. IRAS 09014-4736

This source is also a YSO candidate from Persson & Campbell's (1987) catalogue. They quote a Brγ equivalent width of 9$\pm$3Å consistent with Beck et al. 's (1991) value of 8 ± 2Å, which is just consistent with the figure of 11$\pm$2Å obtained here.

The extinctions derived from the recombination lines and the continuum shortward of 1.5μm are in slight disagreement, suggesting $A_V \simeq 13$ for this object. There is also evidence of a circumstellar infrared excess which translates to a very much higher extinction at $\lambda\lambda > 1.5\mu$m . This is probably attributable to hot dust (see Sect. 3.1 and Table 4). Our data are again at variance with the results obtained for this star by Beck et al. (1991) – they derived an A_V of 26. A review of their data suggests that the Pfγ measurement used in the Brγ/Pfγ flux ratio is the culprit once more. The line flux uncertainty is in this instance $\sim$100%.

3.2.3. IRAS 12389-6147

The visual extinction of IRAS 12389-6147 derived from the HI lines and also the short wavelength continuum are again consistent. For this object, Beck et al. (1991) quote $A_V = 21$, a value that is in good agreement with our measurement ($A_V \simeq 20$, see Table 3). Their evaluation of the reddening used a method due to Rydgren (1976), which is similar to our continuum method.

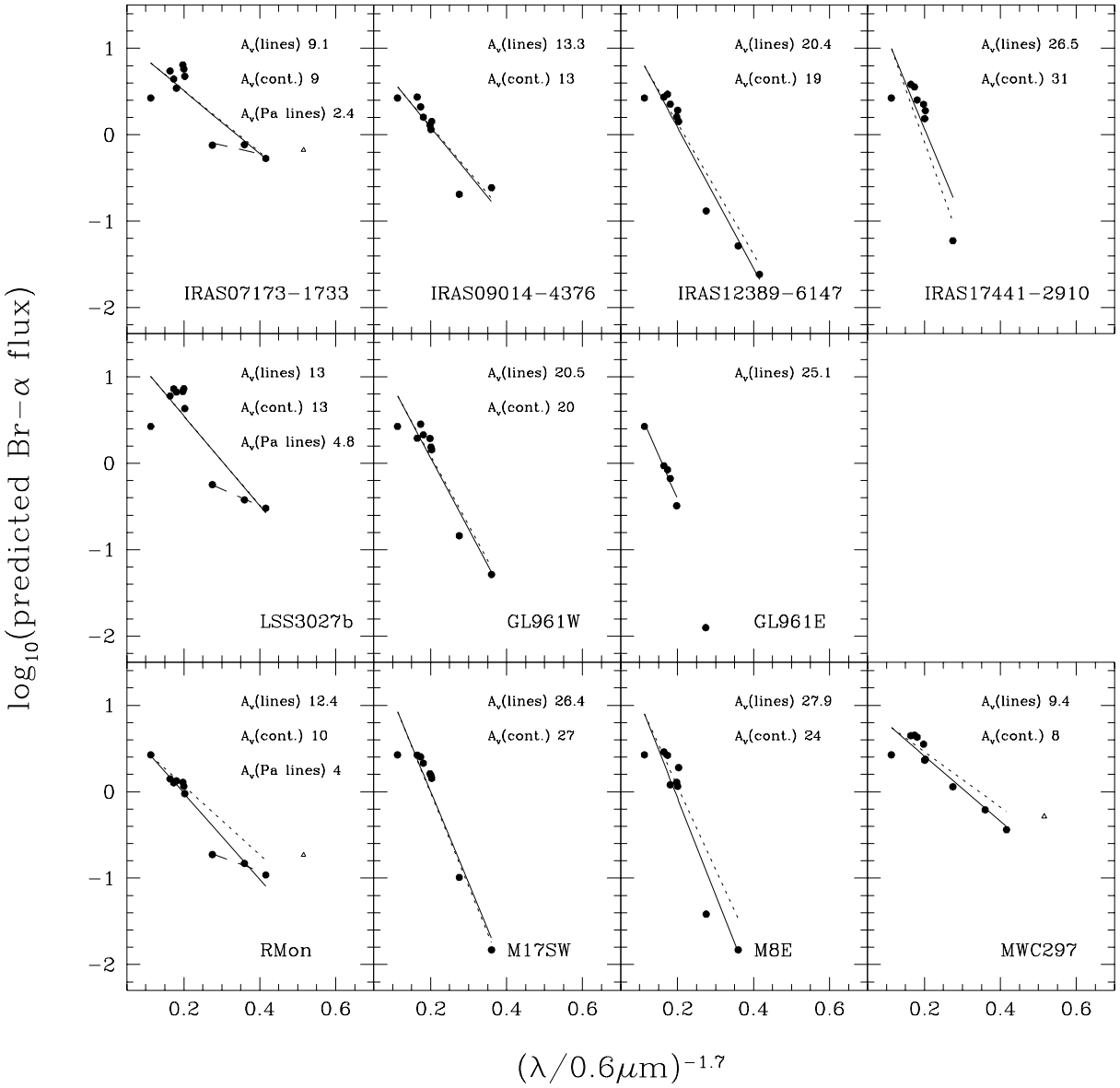

Fig. 3. Target HI recombination line A_V determinations. Each point represents an estimate for the Brα flux given the HI line fluxes in Table 2, (which were normalised to Brγ), and also that Case B recombination ratios apply. If Case B theory applies, all of the points should lie on a straight line, the gradient of which gives the reddening. The solid lines are the fit to all points (except Pa11 where present–see text). The open circles are the data for Pa11, where present. The dotted line is the equivalent locus for the points with A_v derived from the short wavelength continua. For IRAS 07173-1733, R Mon and LSS 3027B the best fit lines from fitting only Paβ, Paγ and Paδ is shown as a dashed line (see text).

Comparison of the Brγ line equivalent width 12 ± 3Å with Persson & Campbell's value of 8 ± 3Å, shows that the new measurement is again just consistent with the earlier. Again this object shows evidence for hot dust emission.

3.2.4. IRAS 14206-6151/1

The spectrum of IRAS 14206-6151/1 shows little evidence for any HI recombination lines. The only line that is clearly identifiable is Brγ, and hence no reddening determination using HI recombination lines is possible. The 'detection' of the line by Persson & Campbell (1987) would seem to be spurious, a conclusion supported by inspection of their published spectrum.

Taken at face value, the two evaluations of the visual extinction from the continuum show scant evidence of any local IR excess emission. However IRAS 14206-6151/1 is one of those objects in which there is a spectral slope change that suggests an excess peaking at much shorter wavelengths than typical of dust at the sublimation temperature. The excess is evident as short as 1.2μm, and contributes $\sim$ 20% of the flux by 1.4μm. The outcome of the crude fit of the spectrum to a combination of starlight and dust emission was $A_V \sim 25$, a slightly higher

value than obtained just by fitting the IJ continuum to reddened starlight. The reason for this small difference becomes obvious on inspection of the dereddened energy distribution in Fig. 2.

3.2.5. IRAS 17441-2910

Compared to the majority of our targets, the HI recombination lines are at low contrast in this object. The visual extinction derived from them is $A_V = 28 \pm 2$ which is nearly consistent with *both* values from the continuum. In this case there is no evidence for any significant local IR emission. The equivalent width of Brγ measured here is 12 ± 1Å again consistent with Persson & Campbell's (1987) value of 10 ± 3Å. CO emission is very well-developed in this source.

3.2.6. LSS 3027B

In this case, the visual extinction of $A_V = 13 \pm 3$ derived from the lines happens to match the continuum value for $\lambda \lesssim 1.5\mu$m seemingly perfectly. However, this has to be compared with Steenman & Thé's (1989) figure of $A_V = 5.97$ for this source (no error given). Their estimate is based on optical and near IR continuum fitting to a reddened Kurucz atmosphere in which it was found advantageous to set R, the ratio of total to selective extinction, equal to 5.1. A high value such as this can be required for sightlines penetrating molecular clouds and so could well be appropriate (see e.g. Cardelli, Clayton & Mathis 1989). Had they imposed a lower value of R closer to the norm for the diffuse interstellar medium, it might very well have led to a yet lower estimate for the visual extinction, rendering the discrepancy even greater.

This difference could be due to the IR excess becoming significant at shorter wavelengths than in other sources. Indeed this is the interpretation implied by Steenman & Thé's fit (see their Fig. 9). Our fitting shows that the excess is already significant ($\sim 20\%$ contribution) at 1.2μm. From the continuum, we derive $A_V \gtrsim 13$ across the whole wavelength range. If this is the correct interpretation, then there is possibly something wrong with the recombination line extinction estimate. (note the large scatter in the Brackett lines in Fig. 3). In this context, it is intriguing to note that, as in the case of IRAS 07173-1733, the Paschen lines alone imply a quite different extinction from that derived on using the Paschen and the Brackett lines together (see Fig. 3): the gradient joining just the Paschen lines corresponds to $A_V = 4.8 \pm 0.3$, roughly in line with Steenman & Thé's value.

These dichotomous results suggest either that this little-known object is a more complicated case than most in this sample, or that the usual absence of an optical detection of the stellar photosphere causes more problems in understanding than we would like to hope. This issue is revisited in the discussion below (Sect. §5).

3.2.7. GL 961E & W

Persson & Campbell (1987) measured the equivalent width of Brγ to be 17 ± 3Å for GL 961 as a whole. The value measured here is 46 ± 5Å for GL 961E, and 16 ± 2Å for GL 961W. The effective equivalent width of both sources added together from our data is ~ 30Å. Clearly there is a large discrepancy between ours and the earlier result. Particularly as this is a double source, the possibility exists that there is more extended emission which is picked up by the larger aperture used by Persson & Campbell. However, this concept is not supported by the K-band images presented by Castelaz et al. (1985). Variability of one or both components may have to be considered.

McGregor et al. (1984) calculated the extinction to GL 961 as a single source to be $A_V = 15.3$ from their 0.6–1.0μm data. In contrast to this, Alonso-Costa & Kwan (1989) derived $A_V = 28 \pm 4$, from flux ratios between the Brα, Brγ and Pfγ lines in the K and L' bands where GL 961E contributes as much and more of the light respectively. The history of this confusing close double source is that it was at first described as single (Cohen 1973), and was only revealed as double by Lenzen et al. (1984) who mapped it in H and K. The separation on the sky is 5.8 arcsec. Castelaz et al. (1985) confirmed this discovery in presenting their own J, H, K, and L maps which show that the eastern component has a very much steeper spectrum than the western component. Castelaz et al.'s interpretation of their own data is that the two sources are associated, that GL 961W is a pre-main sequence star lying above the main sequence, and that GL 961E is a ZAMS B2-B3 star exciting a compact HII region.

It is very striking that the HI Brackett line fluxes we have observed in the eastern component fall very neatly on a straight line in Fig. 3, as would be expected for a relatively straightforward HII region. The flux of Paβ is apparently depressed below the $A_V \simeq 25$ trend. This may be due either to optical depth effects (see §3.2) or to systematic measurement error (merging of the IJ and HK echelle data is less certain in this case because of noise in the IJ data). The reddening of the western component certainly seems to be somewhat less ($A_V \simeq 20$). These results make rough sense in comparison with the previous reddening estimates of McGregor et al (1984) and Alonso-Costa & Kwan (1989). They also sit in a comprehensible relation with respect to the photometric estimates of Hason et al. (1993). Using $J-H$ and $H-K$ colours, they estimated $A_V \sim 15$–20 for GL 961W and $A_V > 30$ for GL 961E. Provisionally, we may conclude that the visual extinction towards GL 961E exceeds that towards the western component by at least 5 magnitudes.

By contrast, Castelaz et al. 's (1985) interpretation assumed that the reddening towards both components was about the same (and of order $A_V \sim 17$, a number that comes primarily from scaling to the 9.7μm silicate optical depth and a ^{13}CO column measurement). The impact of a difference in the reddening towards the two components is that a lower fraction of combined bolometric luminosity (7000 $L_\odot$) should be apportioned to GL 961W than was attributed by Castelaz et al. . This would bring G 961W closer to the main sequence.

From the de-reddened spectra (Fig. 2), it can be seen that both components of GL 961 show the presence of dust (hotter dust in the western component as compared with the eastern).

3.2.8. R Mon

R Mon has recently been identified as a binary with a separation of 0.7" (Close et al. 1997).

The extinction of this object derived from *just* the Paschen lines ($A_V = 3.0 \pm 1$) agrees with the estimate of Kelly et al. (1994) based on the same transitions (see Table 3 and also Fig. 3). It is also in keeping with the optically-based estimates of Cohen & Kuhi (1979) and Hillenbrand et al. (1992). But the trend connecting the higher Brackett and Paschen lines points to a significantly higher extinction ($A_V = 12 \pm 1$). This higher value is not very different from that given by the shorter wavelength continuum ($A_V = 10 \pm 3$). Close et al. (1997) also find a dichotomy in extinction: they calculate $A_V = 13.1$ for $\lambda > 1.28\mu$m and $A_V = 3.6$ for $\lambda < 1.28\mu$m . The situation, in this case, is thus very like that for LSS 3027B and IRAS 07173–1733.

The IR photometry gathered by Hillenbrand et al. shows very clearly that a strong IR excess is associated with this object, as does our fitting which clearly reveals the need for a hot dust component (also see Close et al. 1997). The impact of this on the near-IR energy distribution is readily seen in Fig. 2.

The Brackett lines seen here do not tie in easily with those seen in previous observations. Persson & Campbell (1987) set an upper limit on the equivalent width of Brγ emission line of just 0.8Å, compared to our value of 5 ± 1Å. Evans et al. (1987) were only able to set an upper bound also. Yet, examination of the R Mon spectrum in Fig. 1 shows that Brγ, Br10, Br11 and Br12 are quite distinct and measurable in this object. However, R Mon is known to be seated in extended continuum emission (see Fig. 1 of Close 1997), that is simply scattered light from the central source. Again it is possible that a combination of aperture effects and inaccurate limits on older data can explain the difference.

3.2.9. M17SW IRS1

For this object, McGregor, Persson & Cohen (1984) obtained $A_V \sim 15$ by their continuum and flux ratio methods, whilst Alonso-Costa & Kwan (1989) derived $A_V = 18 \pm 4$ by comparing published Brα Brγ and Pfγ fluxes with their theoretical relation between them. McGregor et al. point out their observation of M17 SW IRS1 was affected by bad seeing – as indeed the poor quality of the resultant spectrum suggests. Their A_v determinations may be unreliable for this reason. The Alonso-Costa & Kwan evaluation is of course dependent on the applicability of their NLTE modelling.

The extinction derived here from both the short wavelength region of the continuum and the HI lines is $A_V \simeq 27$. Again M17 SW shows evidence for a significant hot dust component, but in this instance it only becomes important in the K band.

3.2.10. M8E-IR

Persson & Campbell (1987) measure the Brγ equivalent width to be 1.8 ± 0.3Å as compared to 7 ± 1Å here, which could just be rendered consistent if aperture differences combined with the presence of an extended continuum could be invoked. McGregor, Persson & Cohen (1984) mention that a nebulous patch was observed close to the IR position. However, Bunn, Hoare & Drew (1995) failed to detect any off-source nebulosity, and we did not see any during these observations. Again, we must consider whether or not the Persson & Campbell result is reliable, although they should have been able to detect an equivalent width as large as our reported value. Variability is a strong possibility here (see also Simon et al. 1985).

McGregor, Persson & Cohen (1984) derived $A_V = 15$, while Simon et al. (1985) obtained what they saw as potentially a lower bound of $A_V \sim 21$ on applying a different argument to, effectively, the same data. Bunn et al. (1995) note that mid-IR silicate absorption (Willner et al. 1982) towards M8E-IR suggests much more severe reddening in the region of $A_V \sim 40$. Our estimate based on the HI line flux ratios falls in the middle of this range. However it does seem certain that Brα and Brγ at least, are significantly optically-thick transitions (Simon et al. 1984, Bunn et al. 1995) and so the flux ratio method is not above suspicion. However the difference between the extinctions derived using the HI lines and the shorter wavelength continuum is sufficiently small as to fall within likely error bounds. A visual extinction in the mid to high twenties thus seems reasonable. M8E-IR is another example of an object with a notable red excess contributing at wavelengths as short as 1.5μm. The excess is not consistent in this case with normal dust (defined as $T_d \lesssim 2000$ K, $0 \leq \alpha \leq 2$, Sect. 3.1). In this and in the low contrast of its line spectrum M8E-IR is somewhat similar to IRAS 14206-6151/1.

3.2.11. MWC 297

Hillenbrand et al. (1992) examined the spectral energy distribution of MWC 297. From their Fig. 2d, it can be seen that their dereddened SED becomes significantly different from a Rayleigh-Jeans tail at $\lambda \sim 1.3\mu$m . Hence, the extinction derived from the continuum $\lambda \lesssim 1.5\mu$m should be sound. Indeed the value this yields, $A_V = 8 \pm 3$, is consistent with Hillenbrand et al.'s value of $A_V = 8.3$, and with the continuum determination of $\sim$8 due to McGregor, Persson & Cohen (1984). New data on the blue continuum of this object between 4000 and 5000 Å (Drew et al. 1997) agree with these figures also. Our determination of the extinction from the HI recombination lines ($A_V = 9 \pm 1$) fits into this happy picture as well. Indeed, in this instance the higher Brackett lines, and Paβ, Paγ and Paδ fit well to a single straight line in Fig. 3. Only Brγ and Pa-11 are discrepant. Like M8E-IR and IRAS 14206-6151/1, however, the excess emission cannot be explained in terms of normal dust emission.

3.3. Overview of the HI and continuum determinations of visual extinction

In every case where it has been possible to make the comparison, we find that the visual extinction estimates drawn from the

HI line fluxes and from the shorter wavelength continuum are in satisfactory agreement. If this is a coincidence it is remarkable. Our provisional view is that both methods usually achieve meaningful results.

There are subtleties here, however. In this sample there are three instances in which the decrement from Paβ to Paδ clearly suggests a much lower reddening than implied by the trend joining the Paschen and Brackett lines (R Mon, LSS 3027B and IRAS 07173-1733). Inspection of Fig. 3 reveals that IRAS 09014-4736 may be a fourth example of this. We do not think that optical depth in the Paschen series lines can be the sole cause of this. If it were, we could not then understand the near coincidence between the optically-derived and Paschen line extinctions in both R Mon and LSS 3027B. It is presumably significant that R Mon is well-known to be associated with a substantial compact reflection nebulosity (Close et al. 1997, Jones & Herbig 1982) and with large percentages of on-source linear polarization even at infrared wavelengths (11.1$\pm$0.2 % at J, Minchin et al. 1991, and ~ 8% at H, Close et al. 1997). Our suspicion is that scattered light may be sufficiently dominant in R Mon so as to seriously confuse extinction measurements based on wavelengths in the J band and shortward. Indeed from HST and adaptive optics imaging Close et al. (1997) come to this conclusion. Kelly et al. (1994) expressed concern about this effect also.

As yet, too little is known about the environments of LSS 3027B and IRAS 07173-1733 to assess whether scattering could be a significant effect in these objects as well. The similarities with R Mon hint that it is. Polarization observations of these sources would clearly be helpful.

4. Helium and heavy element spectral lines

*4.1. He*I

The neutral helium lines have been detected at 2.058μm ($2s^1S - 2p^1P^0$) and 1.083μm ($2s^3S - 2p^3P^0$) in some of the sources (see Table 2). The populations of the n=2 levels of neutral helium in a HII region will largely be determined by a balance between ionization and recombination. Collisional excitation from the ground state only becomes significant near the ionization boundary, or perhaps in the post-shock compression due to supersonic outflow colliding with circumstellar material (eg. clumps of natal gas). The upper state of the 1.083μm transition can be collisionally excited from the $2s^3S$ level to give a large flux very readily (see Clegg 1987). Unless the host gas density is low, the population of the metastable 2^3S level will be close to its maximal Boltzmann value. By contrast, the upper level of the 2.058μm line (the singlet equivalent to the 1.083μm line) readily decays to the ground state via the HeI 584Å line (the branching ratio is of the order of 10^3: Weise, Smith & Glennon 1966). Because of this emission in the 2.058μm line is sensitive to optical depth effects in the 584Å line.

A thorough review of the factors involved in the production of emission in the HeI 2.058μm line is given by Shields (1993), who also presents some radiative transfer calculations for its expected flux ratio with respect to Brγ. This ratio can exceed unity in instances where the 2^1P is collisionally pumped. For HII regions of more moderate density ($n_e \sim 10^3$cm^{-3}), the maximum value of the ratio is ~ 0.5 for a stellar effective temperature ~ 40000 K, dropping to around ~ 0.1 for late-O/early-B type exciting stars. In most of the sources where the 2.058μm line is detected with sufficient confidence to warrant measurement, the flux ratio $F(2.058)/F(\mathrm{Br}\gamma)$ is of order 0.1, similar to that seen in LkHα101 (Simon & Cassar 1984). Specifically and in RA order, the reddening-corrected flux ratios are : $F(2.058)/F(\mathrm{Br}\gamma) = 0.034$ (IRAS09014-4736), 0.074 (IRAS12389-6147) 0.33 (IRAS17441-2910) 0.13 (GL961E) 0.16 (GL961W) 0.12 (M17SW).

However, there is an important caveat to be noted. Without resolving the 2.058μm line profile, it is possible in some sources that this flux ratio is affected by the propensity for the 2^1P–2^1S transition to go into absorption. There are already reports of such in S106IR (Drew, Bunn & Hoare, 1993) and in MWC 297 (Murdoch & Drew, 1994). The data on the latter presented here are not of a quality that can add anything to the earlier finding of 2.058μm absorption at just 10% below continuum. It is possible that in the case of M8E-IR alone the 2.058μm line is present as net absorption. However at a resolving power of 400, telluric absorption in the vicinity of this line can confuse its appearance when it is weak.

We find that in IRAS 07173-1733 the 2.058μm singlet transition is not detected, whilst the 1.083μm line is apparent in absorption. Furthermore, an absorption component is clearly present in the 1.083μm feature in the spectrum of LSS 3027B, causing the whole to seem P Cygni-like (Fig. 4). This may be indicative of wind activity but we could also be deceived by the limited spectral resolution of the data – a secure kinematic interpretation of the line profile must await much higher spectral resolution observations.

4.2. Iron lines

Several FeII lines have been observed in most of the targets: 2.091μm , 1.741μm , 1.690μm , 1.070μm , 1.050μm and 0.999μm lines have been detected, together with several other possible identifications. Embedded YSOs and Be stars both exhibit the 0.999μm line (McGregor, et al. 1984) which arises from the same multiplet as the 1.113μm line although this second line is not detected in any of the present spectra. The 2.091μm line is seen in BN (Scoville et al. 1983) and also in LkHα101 (Simon & Cassar 1984). The 1.690μm line may be FeII, OI or CI, although if the 2.091μm line is present, then the 1.690μm line is likely to be FeII as it arises from the same multiplet.

In principle, ratios among the FeII lines may have some power as diagnostic indicators for the local environment. Unfortunately, the processes that pump these lines are sufficiently complex that no simple conclusions can be made as yet concerning the exact nature of the source of this emission (cf. the discussion in Hamann et al. 1994 of FeII emission in η Carinae). Upper levels of all of these lines could be populated by HI Lyα (Johansson & Jordan 1984) or Balmer continuum flu-

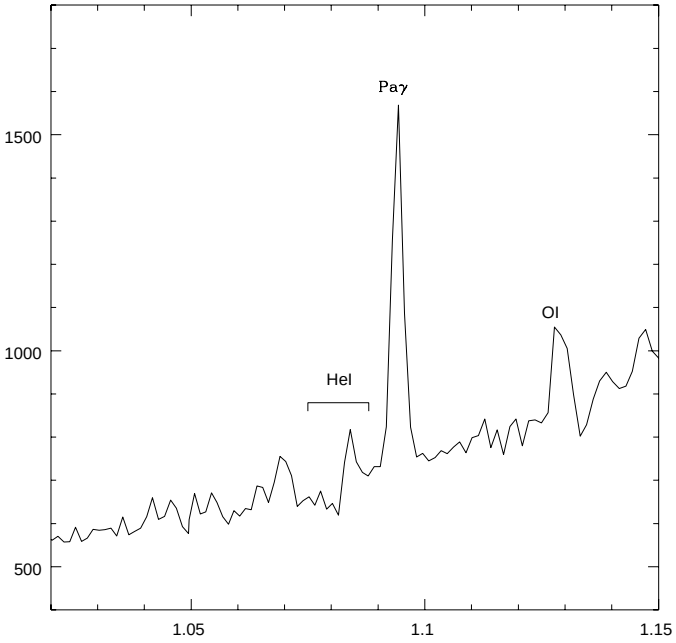

Fig. 4. LSS 3027B HeI1.083μm line exhibiting a lineshape similar to the wind formed P Cygni lineshapes (see text).

orescence (Lucy 1995), either directly or through secondary processes. The situation is further complicated by the fact that at the densities required for efficient fluorescence ($n_e > 10^5$ cm^{-3}, in order that metastable levels above the ground state might be well populated), collisional excitation might also become significant (Bautista, Peng & Pradhan 1996). However, the very existence of the IR permitted lines in the majority of our targets would seem, at the very least, to point to relatively high densities. In the past it has been suggested that a partially-ionized zone (the ionization potential of Fe^+ is 7.87 eV) in a circumstellar disk might provide the right conditions for the creations of such lines (Hamann et al. 1994, also see Lopes et al. 1992). The one peculiar object that shows FeII emission then is GL961E, which we otherwise identify as a potentially normal HII region powered by a B star. The presence of the FeII lines may indicate that although the much of the emission is from an HII region, the object is still rather young and in possession of a dense circumstellar medium.

In IRAS 12389-6147 and R Mon, and perhaps in GL961W and M17SW, the forbidden transition [FeII] $a^6D_{9/2} - a^4D_{7/2}$ at 1.257μm is seen. In IRAS 12389-6147 the [FeII] $a^6D_{3/2} - a^4D_{5/2}$ transition at 1.3278μm may also be present. The weakness of these lines is consistent with them arising in a lower-density partially-ionised zone around the H^+ region The ratios of the $a^6D_{9/2} - a^4D_{7/2}$ line with HI Paβ are consistent with those found in HII regions (eg. Lumsden & Puxley 1996). If the $a^6D_{3/2} - a^4D_{5/2}$ transition possibly detected in IRAS 12389-6147 is real, it further indicates a larger density for this zone than in the other objects (the observed ratio of the two [FeII] lines implies a density of $\sim 10^4$cm^{-3}). However, a density this large implies that we should see other [FeII] lines that are not obviously present. Given the proximity of the 1.3278μm line to the edge of the atmospheric window, it is likely that we have overestimated the strength of this line. That apart, the lack of other [FeII] lines in the objects indicates relatively moderate densities, $n_e \sim 10^3$cm^{-3}, in the partially ionised zone.

4.3. OI

Two OI lines are detected in several spectra at 1.316μm and 1.128μm . Both can be due to fluorescence but not by the same route. On the one hand, a coincidence between Lyβ 1025.72Å and the OI 1025.76Å line can promote a cascade in which lines at 1.128μm , 8446Å and 1302Å are emitted (for this to work most effectively, strong velocity gradients should not shear the Lyβ emitting gas from the OI recipient). On the other, continuum fluorescence gives rise to the 1.316μm line. The absence of strong emission in the 0.927μm recombination line in any of the objects suggests that very little of the OI emission is being produced by recombination. In an HII region most of the oxygen will be ionized (Grandi 1980) and hence fluorescent OI emission is more likely to arise in or beyond an ionization front. The flux ratio between these two OI lines, $F(1.128)/F(1.316)$, ranges from 0.1 for UV continuum fluorescence with Lyβ in absorption, up to 6.2 in the case that Lyβ is infilled to the UV continuum level (Grandi 1975). If the ratio exceeds 6.2 then the OI emission excitation mechanism is dominated by Lyβ fluorescence.

There is clearly significant overlap between the mechanisms giving rise to OI and FeII emission. Hence, where FeII is detected, it is reasonable that OI should also be seen. The converse need not be true however, since the OI fluorescence works out of the ground state, and so can occur even if the circumstellar density is low. Previous work on HII regions and planetary nebulae indicate no consistent trend as to whether or not particular types of objects show evidence for either UV continuum or Lyβ fluorescence, although continuum fluorescence appears to be more common.

We provide the reddening-corrected OI $F(1.128)/F(1.316)$ ratios in Table 4. Only IRAS 14206-6151/1 and IRAS 17441-2910 show no detectable OI emission at either 1.316μm or 1.128μm . The lines are also too weak or signal-to-noise ratio too poor in GL 961E, GL 961W, M8E-IR and M17SW IRS1 to say anything conclusive. In IRAS12389−6147, MWC 297, LSS 3027B and R Mon, both lines are detected and yield ratios of 13, 8, 7 and ~ 6 respectively, all ratios consistent with Lyβ fluorescence. However for R Mon and LSS 3027B, where it is likely that scattered light contributes significantly to the short wavelength spectrum, there has to be some concern that the flux of the 1.128μm line might be somewhat inflated. The upper limits for detection of the 1.316μm line in IRAS 09014−4736 indicate that UV continuum fluorescence is the dominant mechanism there, hinting either at the quenching of the Lyβ fluorescence by velocity shear or at formation in a less dilute stellar radiation field.

4.4. CO

Confirmation of the identification of the CO bandheads is provided by the fact that the emission appears asymmetric with emission trailing longward of the band head (see Chandler et al. 1993). From observations of BN, Scoville et al. (1983) show that CO band emission implies warm, dense, neutral gas existing within BN's line emitting envelope. CO emission requires reasonably high temperatures (a few 1000K) and densities $n \gtrsim 10^{10}\mathrm{cm}^{-3}$ (Scoville et al. 1983, Geballe & Persson 1987, Carr 1989). The CO emitting region may therefore be interior to the dust destruction zone at T~ 1500K. Band emission $J = 2 \rightarrow 0$ is detected in three objects in our sample. The target showing CO most clearly is IRAS 17441-2910.

*4.5. Na*I

Sodium has an ionization potential of 5.1eV so it will be mostly ionized in the HII region. The 2.206/9μm lines are fluorescent, pumped by 3300Å photons (Thompson & Boroson 1977, see also Scoville et al. 1983). If these lines are observed in emission, sodium must be relatively underionized and hence shielded from the direct stellar radiation field. The 2.206/9μm emission may arise beyond an ionization front in the flow where 3300Å photons can travel upstream and excite the neutral sodium. It is also possible that NaI may exist and be appropriately excited in a circumstellar disc, where it can be shielded from the direct stellar photon field.

NaI emission may arise in similar physical conditions to those needed for CO band-head emission. NaI emission is probably present in all objects where CO emission has been detected, although in IRAS07173-1733 where CO emission is not seen, NaI is present and measurable.

5. Discussion and conclusions

In this paper we have presented a modest sample of YSOs that are all likely to fall at the top end and perhaps extend somewhat the luminosity range presented by Herbig Be stars (up to $\sim 10^4 \mathrm{L}_\odot$). A key result of this study is the large measure of success achieved in reconciling different measures of the visual extinction. Ultimately this is attributable to the wide wavelength coverage of the relatively flux-calibrated IRIS spectra at our disposal – we have been able to combine hydrogen recombination line data spanning the I, J, H and K windows with measurements of the continuum slope in IJ. That these two methods agree is very reassuring. Those cases where the derived extinctions have to be doubted (R Mon, LSS 3027B and IRAS 07173−1733) are flagged by our data in that there is plain evidence of a Paschen line decrement at odds with the trend obtained on bringing the Brackett lines into consideration as well. In effect, data spanning such a wide wavelength range, and a range in which it is a reasonable expectation that at most only a part of it is liable to significant scattered light contamination, offers its own internal check.

A basic challenge presented by massive YSOs is the construction of a classification scheme that will reflect evolutionary stages even in the presence of confusing environmental effects. Potential components of such a scheme might be the magnitude of the 1.5–2.0μm circumstellar continuum emission, the line/continuum contrast and the lines themselves. Classifying an individual source using these components has been attempted before (see below), although each method does have its own advantages, disadvantages and possible pitfalls.

The diagnostic near-IR colour-colour plots presented by Lada & Adams (1992) in their discussion of HAeBe stars attempt to classify in effect from the continuum emission. These authors viewed a high value of $H-K$, relative to the combination of $J-H$ and $H-K$ producible by reddening of a Rayleigh-Jeans law, as evidence of a circumstellar accretion disk. The alternative view, that such an excess may provide evidence for grain processing, has been argued by Hartmann, Kenyon & Calvet (1993). These opposing interpretations of the same phenomenon carry different implications. For example, attribution of the near-IR excess to emission from small hot dust grains does allow that younger more deeply embedded objects need not exhibit an $H-K$ excess, in that larger dust grains more typical of undisturbed molecular clouds can be expected to produce excesses peaking at $\lambda \sim 4-5\mu\mathrm{m}$. By contrast, one should expect an $H-K$ excess to continue to be apparent in younger objects if optically-thick continuum emission from an accretion disk is responsible for it. Lada & Adams (1992) supported this view in pointing out that younger Class I sources lay to the right of more-evolved Class II in their $J-H$ versus $H-K$ diagrams.

$J-H$ and $H-K$ colours have been published for most of our targets, and reveal an $H-K$ excess with respect to the reddening locus – indeed Persson & Campbell (1987), from whose paper some of our sample are drawn, used this criterion to select candidate YSOs from the IRAS PSC in the first place. This, in effect, is a re-expression of the results we have plotted in Fig. 2 and, at first, sight fits in with the picture of Lada & Adams. However there are instances that warn that the magnitude of the continuum excess is an unreliable indicator of youth when applied to individual objects. For example, the deeply embedded source IRAS 17441−2910 exhibits almost no excess longward of $\sim$1.5μm , while MWC 297 shows a very marked one. Without further information one might be tempted to conclude that MWC 297 is the younger source. Yet, on the basis of these objects' spectra, as well as their overall reddening, there is certainly a case to be made that MWC 297 is approaching the end of its early evolution (see also Drew et al. 1997) while IRAS 17441−2910 can be argued, tentatively, on the basis of its CO emission to still be in possession of an extensive cool circumstellar disk (see the discussion of high resolution CO spectroscopy in Chandler et al. 1993). There are also cases here, such as R Mon, where a substantial scattering component in the energy distribution may confuse conclusions based on $J-H$,$H-K$ colours.

At the bolometric luminosities associated with late-O/early-B stars, it is more likely that the near-IR continuum excess is due to small dust grains, rather than to emission from continuing accretion. This is not intended to imply that accretion has

Table 4. Summary of spectral characteristics. A_V for each object is that calculated from HI recombination lines (for IRAS1420-6151/1 the value is that derived from the continuum $\lambda \lesssim 1.5\mu$m). For HeI, "a" stands for present in absorption, "e" for emission, crosses in the other columns indicate the presence of an emission component, whereas "?" indicates weak evidence for that feature. In the penultimate column, summarising the nature of the IR excesses seen, a "?" indicates the presence of a significant IR excess of unknown type. Final column: HBe = Herbig Be star, BN = BN-type object, HII = compact HII region. We use the term 'Herbig Be' to designate more evolved YSOs, while the term 'BN-type' labels putatively younger, deeply embedded sources.

Source	A_V	Brγ EW (Å)	HeI	OI flux ratio F(1.13μm /1.32μm)	[FeII]	FeII	CO	NaI	IR excess	Class
IRAS 0717	9±2	6 ± 2	a	high		x		x	hot greybody	HBe
IRAS 0901	13±2	11 ± 2		low		x			hot greybody	HBe
IRAS 1238	20±2	12 ± 3		13	x	x		?	hot greybody	HBe
IRAS 1420	(23±3)	2 ± 1							dust+HII wind?	BN
IRAS 1744	27±3	12 ± 1	e	~ 0		x	x	x	negligible	?
LSS 3027B	13±3	10 ± 4	e	7					dust+HII wind?	HBe
GL 961W	21±3	16 ± 2	e		?	x	x	?	hot greybody	BN/HBe
GL 961E	25±3	46 ± 5	e			x			cool greybody	HII
R Mon	12±1	5 ± 1		6:	x	x		x	hot greybody	HBe
M17SW IRS1	26±3	28 ± 5	e	3	x	x		?	hot greybody	HBe
M8E-IR	28±4	7 ± 1				x	?	?	dust+HII wind?	BN
MWC 297	9±1	50 ± 2	e	8					dust+HII wind?	HBe

necessarily ceased in these objects – only that it is not feasible to detect it as an additional component on top of the stellar continuum. This is because the extra light due to an accretion disk would not introduce a break in spectral slope between 0.9 and 2.5μm unless the disk inner radius is substantially larger than the stellar radius (see Kenyon & Hartmann 1987) – its presence would, however, on application of the Rayleigh-Jeans assumption lead to slightly inflated reddening estimates. It is therefore plausible that the detectable excess emission at $\sim$2 μm (as signalled by a break in spectral slope at shorter wavelengths) might actually increase with time during the early evolution of these luminous stars – as an initial population of large dust grains are processed into smaller grains, capable of achieving higher temperatures via thermal-spiking, via the action of the central star's radiation field. A complicating factor, inevitably, is that environment must play a role in this – where the reservoir of dust is larger and more uniformly distributed around the young star, a stronger IR excess is likely.

Returning to the problem of classifying individual objects, we now consider the extent to which the line spectrum can help. The work of others (see Sect. 4.4) leads to the impression that CO emission can be a reasonably reliable tracer of circumstellar gas in a low ionization state on the scale of a few 10s of R_*. Furthermore, as commented above, it may well be seated in a circumstellar disk. Yet it should not be regarded as an unambiguous indicator of youth – given that evolved B[e] stars can also be CO emitters (McGregor et al. 1988). However, assuming that other factors such as location identify an embedded source as young rather than post main sequence, it would seem that CO emission is more likely to be linked with the genuinely embedded phase rather than the later phase in which the young star has more completely ionized its surroundings.

Unfortunately it is well-established that only a minority of deeply embedded sources are CO emitters (Carr 1989): this implies that it is only the presence of the emission that is of diagnostic value – not its absence. For example, we do not detect it in IRAS 14206−6151/1, an object that otherwise qualifies as BN-type. In this case we propose that the low contrast of its line spectrum with respect to the continuum is indicative, as well its considerable reddening ($A_V \sim 23$). The basis for associating youth with contrast of line spectrum is simply that one might expect a higher contrast line spectrum to develop as the emitting nebulous volume increases in response to the young star's increasing excavation and ionization of its environment. A limiting example of this here is the object GL 961E, already labelled as an HII region, in which the line contrast is enormous. In this context it is relevant to note that the high contrast line emission seen in such sources as LkHα 101 and S106IR is likely to be composite in origin (Simon & Cassar 1984; Drew, Bunn & Hoare 1993) – the narrow and bright emission line cores may be due to circumstellar nebular emission while only the broad low contrast line wings are directly attributable to stellar outflow. There is still work to do on this in that a detailed and compelling explanation for the line emission produced in any one object has yet to be forthcoming (e.g. see the discussion of MWC 297, another very high contrast line emitter, in Drew et al. 1997).

In producing a summary table of the spectral properties of our sample of objects (Table 4), we have included tentative object classifications. Our prescription for doing this places greater emphasis on the nature of the $\sim$2μm continuum excess as revealed by our simplified fitting (Sect. 3.1) than on its magnitude. The contrast of the line spectrum and also the presence of particular features such as CO is taken into account also. Most of our sample conforms to the anti-correlation between visual extinction and emission line contrast that would be expected if the former crudely decreases and the latter increases with age. An object that goes against this, in combining high line contrast (as measured in terms of Brγ equivalent width) with high reddening, is M17SW IRS1. This may be an example of a source in

a misleading location in that it could be behind the SW obscuration of M17 (eg. Gatley et al. 1979, Wang et al. 1993) but is not actually embedded in it. It was also suggested by Bunn, Hoare & Drew (1995), on the basis of its spectrally-resolved IR HI line profiles, that this object stands apart from typical BN-type objects. This is why we have labelled it in Table 4 as 'BN/HBe' – it has in the past been labelled as a BN-type object, while we surmise it is a concealed Herbig Be star. Otherwise, our labelling of the better-known sources coincides with earlier classifications.

Finally we draw attention once more to the suggestion concerning many objects in our sample that IR spectral variability may have been uncovered (Sect. 3.3). Optical variability is certainly well documented for Herbig Be stars (e.g. the catalogue of Thé, de Winter & Pérez 1994) but is less commonly recognised at IR wavelengths in either this class or among the BN-type objects (exceptions to this are the study by Nisini et al. 1994 of NGC 2024 IRS2, and the study of M8E-IR by Simon et al. 1985). In the future this is an issue that deserves much more attention than hitherto.

References

Alonso-Costa J.L, Kwan J., 1989, Ap.J., 338, 403
Beck S.C, Fischer J., Smith H.A., 1991, Ap. J., 383, 336
Becklin E.E., Neugebauer G., 1967, ApJ, 147, 799
Bally J., Lada C.J., 1983, ApJ, 265, 824
Bautista M.A., Peng J., Pradhan A.K. 1996, ApJ, 460, 372
Bunn J.C., Hoare M.G., Drew J.E., 1995, MNRAS, 272, 346
Cardelli, J.A., Clayton G.C., Mathis J.S., 1989, ApJ, 345, 245
Carr, J.S., 1989, ApJ, 345, 522
Castelaz M.W., Grasdalen G.L., Hackwell J.A., Capps R.W., Thompson D., 1985, Astron. J. **,** 90, 1113
Chandler C.J., Carlstrom J.E., Scoville N.Z., Dent W.R.F., Geballe T.R., 1993, Astrophys. J. Lett. **,** 412, L71
Clegg R.E.S., 1987, MNRAS, 229, 31
Close L.M., Roddier F., Hora J.L., Graves J.E., Northcott M., Roddier C., Hoffmann W.F., Dayal A., Fazio G.G., Deutsch L.K., 1997, ApJ, in press
Cohen M., 1973, Astrophys. J. Lett. **,** 185, L75
Cohen M., Kuhi L.V., 1979 Ap.J.Supp., 41, 743
Drew J.E., Bunn J.C., Hoare M.G., 1993, MNRAS, 265, 12
Drew J.E., Bushfield G., Hoare M.G., Murdoch K.A., Nixon C.A., Oudmaijer R.D., 1997, MNRAS, 286, 538
Evans N.J., Levreault R.M., Beckwith S., Skrutskie M., 1987, ApJ, 320, 364
Gatley I., Becklin E.E., Sellgren K., Werner M.W., 1979 ApJ, 233, 575
Geballe T.R., Persson S.E., 1987, ApJ, 312, 297
Grandi S.A., 1975, ApJ, 196, 465
Grandi S.A., 1980, ApJ, 238, 10
Gunhathakurta A., Draine B., 1989, ApJ, 345, 230
Hanson M.M., Geballe T.R., Conti P.S., Block D.L., 1993, A&A, 273, L44
Hamann F., DePoy D.L., Johansson S., Elias, J., ApJ, 422, 626
Hartmann L., Kenyon S.J., Calvet N., 1993, ApJ, 407, 219
Herbig G., 1962, *Adv. Astron. & Astrophys.*, 1, 47
Hillenbrand L.A., Strom S.E., Vrba F.J., Keene J., 1992, ApJ, 397, 613
Howarth I.D., 1983, MNRAS, 203, 301
Hummer D.G., Storey P.J., 1987, MNRAS, 224, 801
Johansson S., Jordan C. 1984, MNRAS, 210, 239
Jones B.F., Herbig G.H., 1982, Astron. J. **,** 87, 1223
Kelly D.M., Rieke G.H., Campbell B., 1994, Ap.J., 425, 231
Kenyon S.J., Hartmann L., 1987, ApJ, 323, 714
Koornneef J., 1983, A&A, 128, 84
Kurucz R.L., 1991, in *Precision Photometry: Astrophysics of the Galaxy*, ed. A.C. Davis Philip, A.R. Upgren, K.A. James, Schenectady:Davis, p 27
Lada C.J., Adams F.C., 1992, ApJ, 393, 278
Lenzen R., Hodapp K.-W., Reddmann T., 1984, A&A, 137, 365
Lopes, D.F., Damineli Neto A., de Freitas Pacheco J.A., 1992, A&A, 261, 482
Lucy L. B. 1995, A&A, 295, 555
Lumsden S.L., Puxley P.J., 1996, MNRAS, 281, 493
McGregor P.J., Hyland A.R., Hillier D.J. 1988, ApJ, 324, 1071
McGregor P.J., Persson S.E., Cohen J.G., 1984, Ap J., 286, 609
Minchin N.R., Hough J.H., McCall A., Aspin C., Yamahita T., Burton M.G., 1991, MNRAS, 249, 707
Murdoch K.A., Drew J.E., 1994, in The Nature and Evolutionary Status of Herbig Ae/Be Stars, ASP Conference Series, 62, ed. P.S. Thè, M.R. Perez and E.P.J. van den Heuval, p. 377
Nisini B., Smith H.A., Fischer J., Geballe T.R., 1994, A&A, 290, 463
Persson S.E., Geballe T.R., McGregor P.J., Edwards S., Lonsdale C.J., 1984, ApJ, 286, 289
Persson S.E., Campbell B., 1987, Astron. J. **,** 94, 416
Rydgren A.E., 1976, *PASP*, 88, 111
Scoville N., Kleinmann S.G., Hall D.N.B., Ridgway S.T., 1983, ApJ, 266, 623
Simon M., Felli, M., Cassar L., Ficsher J., Massi M., 1983, ApJ, 266 623
Simon M., Cassar L., 1984, ApJ, 283, 179
Simon M., Peterson D.M., Longmore A.J., Storey J.W.V., Tokunaga A.T., 1985 Ap. J. 298 328
Shields J.C., 1993, ApJ, 419, 181
Shu F.H, Adams F.C., Lizano S., 1987, Ann. Rev. Astr. Astrophys. **,** 25, 23
Smith H.A., Fischer J., Geballe T.R., Schwartz P.R., 1987, ApJ, 316, 265
Steenman H., Thè P.S., 1989, Ap. Sp. Sci., 161, 75
Thè P.S., de Winter D., Perez M.R., Astr. Astrophys. Supp. Sers. **,** 104, 315
Thompson R.I., Boronson T.A., 1977, Astrophys. J. Lett. **,** 216, L75
Thompson R.I., 1982, ApJ, 257, 171
Wang Y., Jaffe D.T., Evans N.J. Hayashi M., Tatematsu K., Zhou S., 1993, ApJ, 419, 707
Weise W., Smith M., Glennon B., 1966, *Atomic Transition Probabilities*, BSRDS-NB5, 4
Willner S.P., Gillett F.C., Herter T.L., Jones B., Krassner J., Merrill K.M., Pipher J.L., Puetter R.C., Rudy R.J., Russell R.W., Soifer B.T., 1982, ApJ, 253, 174
Wright, A. E., Barlow, M. J., 1975, MNRAS, 170, 41
Yorke H.W., 1985, *Mit. Astro. Ges.*, 63, 89